

Research papers

# A novel approach to estimate the state of charge for lithium-ion battery under different temperatures incorporating open circuit voltage online identification



Xiao Renxin <sup>a</sup>, Hu Yanwen <sup>a</sup>, Zhang Wei <sup>a</sup>, Chen Zhaojun <sup>b,\*</sup>

<sup>a</sup> Faculty of Transportation Engineering, Kunming University of Science and Technology, Kunming 650500, China

<sup>b</sup> City College, Kunming University of Science and Technology, Kunming 650224, China

---

## ARTICLE INFO

### Keywords:

Lithium-ion battery  
SoC  
Closed-loop estimation  
Open circuit voltage  
Adaptive unscented Kalman filter (AUKF)

---

## ABSTRACT

The open circuit voltage (OCV) is inherently related to the state of charge (SoC) and their relationships under different temperatures are crucial for accurate SoC estimation for the lithium-ion battery based on the equivalent circuit model (ECM), which requires long time-consuming offline OCV tests. In this research, an online closed-loop SoC estimation without conducting OCV tests is put forward. Firstly, the parameters of the Thevenin model for the lithium-ion battery are identified online through the adaptive recursive least square with forgetting factor (AFFRLS). Afterwards, the adaptive unscented Kalman filter (AUKF) is applied to achieve the online closed-loop SoC estimation with the identified parameters. Subsequently, the relationships between the OCV and SoC under different temperatures have been reconstructed online. The proposed method is validated under different temperatures. The research reveals this method can accurately estimate the SoC and is robust to the initial SoC values in wide temperature range.

---

## 1. Introduction

### 1.1. Technical background and challenges

The battery management system (BMS) of lithium-ion battery is crucial for the electric vehicle. It plays a vital role in monitoring the battery status, ensuring its safety and extending its service life [1,2]. State of charge (SoC) is one of the critical parameters of the BMS, which is the premise of the rational use of the battery. Therefore, the accuracy SoC is important for the BMS and the energy management of the vehicle [3]. Lithium-ion battery is a strong nonlinear and time-varying system. It is difficult to directly observe the SoC due to the complex internal electrochemical reaction [4]. In addition, the ambient temperature can affect the SoC estimation. In order to estimate the SoC accurately, a large number of experiments or tests have to be conducted to set up the model for the lithium-ion batteries, which will cost a lot of time and money [5]. This makes accurate SoC estimation a big challenge. Accordingly, this research puts forward the adaptive recursive least square with forgetting factor (AFFRLS) to identify the parameters of the equivalent circuit model (ECM) for the lithium-ion battery online and utilizes a closed-loop filter to estimate SoC without conducting the open circuit voltage (OCV)

tests, which will accomplish the SoC estimation online without requiring lots of offline experiments and tests.

### 1.2. Review of literature

#### 1.2.1. SOC estimation review

Many scholars have conducted SoC estimation and achieved many research findings. Currently, there are three main categories of the SoC estimation for the lithium-ion batteries: the direct measurement method [6], the big data-driven method [7] and the model-based method [8].

The direct measurement method includes the OCV method [6,9] and ampere-hour (Ah) integral [10,11] method. The OCV method can exactly estimate the SoC value under non-operating conditions, where the battery must be rested for a long period to obtain the OCV [12,13], and then the corresponding SOC is attained by inferring the OCV-SoC relationship. The Ah integral method can satisfy the real time problem, however, it is deeply influenced by the initial SoC error and the measurement error, which results in the accumulated error as the time increases leading to low estimation accuracy. The OCV method and the Ah integral method are open-loop estimation methods, which cannot be corrected with the measurement feedback. It is hard to accurately

---

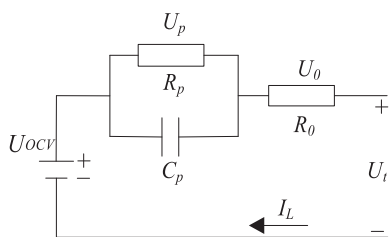
\* Corresponding author.

E-mail address: [huzhisheng111@qq.com](mailto:huzhisheng111@qq.com) (C. Zhaojun).

**Table 1**

Comparisons of different methods for the SoC estimation.

Methods		Advantages	Disadvantages
Direct measurement method	OCV method Ah integral method	High accuracy Easy implementation	Depending on offline OCV tests Sensitive to initial SoC and ambient noise
Data-driven method	NN Learning machine	Approximating arbitrary complex nonlinear system Strong robustness and fault tolerance Few parameters need to be learned Adapt to scenarios with small data volume	High requirements for huge data and hardware performance High dependence on feature engineering
KF algorithm method	AEKF  AUKF	Closed-loop estimation Adaptively updating the noise covariance  Closed-loop estimation Adaptively updating the noise covariance The derivatives of the state function and measurement function are not required	High requirements for model accuracy The derivatives of the state function and measurement function are required High order items are omitted when linearizing the nonlinear system High requirements for model accuracy Calculation amount is greater than AEKF

**Fig. 1.** The circuit diagram of the Thevenin model.**Table 2**

The implementation of the AFFRLS.

Initialization: $\theta_0, \lambda_0, K_0, P_0$ .
Step 1: Updating priori parameter and covariance matrix:
$\hat{\theta}_k^- = \hat{\theta}_{k-1}^+, P_k^- = P_{k-1}^+$
Step 2: Updating the gain $K$
$K_k = \frac{P_k^- \varphi_k}{\lambda + \varphi_k^T P_k^- \varphi_k}$ $P$ is the covariance matrix
Step 3: Calculating the terminal voltage
$U_k = \varphi_k \hat{\theta}_k^-$
Step 4: Calculating the estimation error of the terminal voltage
$e_k = y_k - U_k$ Herein, $y_k$ is the measured terminal voltage.
Step 5: Updating the estimated parameter vector
$\hat{\theta}_k^+ = \hat{\theta}_k^- + K_k e_k$
Step 6: Updating the covariance matrix
$P_k^+ = \frac{P_k^- - K_k \varphi_k^T P_k^-}{\lambda_k}$
Step 7: Updating the forgetting factor
$\begin{cases} \lambda_k = \lambda_{\min} + (1 - \lambda_{\min}) h^{k_*} \\ \gamma_k = \text{round}\left(\left(\frac{e_k}{e_{\text{base}}}\right)^2\right) \end{cases} \quad (10)$

estimate the SoC online.

With the rise of big data techniques and platforms, the big data-driven based SoC estimation has attracted great attention from researchers. This method adopts the neural network (NN) [7] or learning machine to map the measured data into SoC. In [14] only a small amount of discharge data is needed to predict the SoC with a trained NN model which requires a large amount of experimental data for training, and the estimation results are influenced by the sample data. In [15] the voltage, current and temperature are input to the Elma network to predict the SoC and it achieves good accuracy. In [16] an improved gate recurrent unit (GRU), which solves the gradient disappearance and high calculation of the traditional NN, to estimate the SoC. In [17] a particle swarm optimization (PSO) optimized long short-term memory (LSTM) is proposed to estimate SoC and solves the problem of manual setting of parameters of traditional LSTM thereby improving the estimation accuracy. In [18] deep recursive kernel technique is used to improve the gaussian process regression (GPR) to make sorting and recursive structure of the captured data better. The results reveal this method has good predication accuracy of the SoC. In [19] the currents, voltage and temperatures of the charging and discharging process are applied to set up the support vector machine (SVM) to estimate the SoC. The results verify that the model can accurately and quickly predict SoC with appropriate training sets and radial basis function (RBF) as the kernel function. Those big data-based methods require mass data collected from offline experiments or field application to train the NN or learning machine. Moreover, the prediction accuracy depends on the completeness and accuracy of the training data sets [20].

The model based methods have been widely used [8]. The representative algorithms are fuzzy logic (FL) method [21,22], and filter-based algorithm [23], etc. The FL method simulates fuzzy thinking and reasoning ability of mankind to estimate the SoC, but this method requires a high level of engineering experience and a large amount of experimental data. The filter-based algorithms such as the sliding mode observer [24](SMO), the Luenberger observer, the Kalman filter (KF) estimate the SoC based on its dynamic model, among which the KF uses an iterative computation to attain the best solution in term of minimum variance and has been extensively used. This kind of algorithm has a small calculation cost, and it is suitable for SoC estimation online. Moreover, these filter-based algorithms have a closed-loop characteristic, which makes it easier to deal with various uncertainties [25].

To improve the SoC estimation accuracy of the traditional KF algorithm, many scholars conduct a lot of researches to make the KF-like algorithms better for SoC estimation. For example, the extended KF (EKF) can resolve the nonlinear system with its first order Taylor series [26]. In [27] the EKF is leveraged to estimate the SoC, which has a good estimation accuracy, but it ignores the second-order and higher-order terms in the process of linearizing the model by first-order Taylor series resulting in inevitable linearizing errors that affects the estimation accuracy [28]. The unscented KF (UKF) [29] utilizes the recursive unscented transform (UT) technique to approach the observed target without system linearizing approximation. For strongly nonlinear systems, the UKF has higher estimation accuracy and better robustness than the EKF [30]. However, the UKF is prone to be disturbed by unknown noises that causes inaccurate estimation [31]. In [31,32] the adaptive UKF (AUKF) and adaptive EKF (AEKF) are adopted to estimate the SoC, which can update the process noise covariance and the measurement noise covariance online to improve the accuracy and stability of the estimation.

The advantages and disadvantages of these three typical methods are compared and presented in Table 1. The AUKF is a kind of closed-loop method and can adaptively update the covariances of the process noise and the measurement noise. In addition, the AUKF does not require derivatives of the state function and the measurement function and has no approximation errors for the strong nonlinear system. Therefore, the AUKF is adopted to estimate the SoC for the lithium-ion battery in this research.

**Table 3**

The SOC estimation based on the AUKF algorithm.

Step 1: Initializing state  $x_0$  and covariance matrix  $P_0$ :

$$\begin{cases} \bar{x}_0 = E(x_0) \\ P_0 = E[(x_0 - \bar{x}_0)(x_0 - \bar{x}_0)^T] \end{cases}$$

Step 2: Generating the sigma of the sampling point and calculating the weighted value:

(1) Generating sigma point at the  $k$ th sampling moment as follows,

$$\begin{cases} x_0 = \hat{x}_{k-1} \\ x_{i,k-1} = \begin{cases} \hat{x}_{k-1} + (\sqrt{(L+j)P_{k-1}})_i, & i = 1, 2, \dots, L \\ \hat{x}_{k-1} - (\sqrt{(L+j)P_{k-1}})_i, & i = L+1, L+2, \dots, 2L \end{cases} \end{cases}$$

where  $L$  is half of the number of the sigma points.

(2) Calculating the weighted value as follows,

$$\begin{cases} w_0^m = \frac{j}{L+j} \\ w_0^c = \frac{j}{L+j} + (1 - \alpha^2 + \xi) \\ w_i^m = w_i^c = \frac{1}{2(L+j)}, & i = 1, 2, \dots, 2L \end{cases}$$

where  $j$  is the size coefficient expressed as  $j = \alpha^2(L + \kappa)L$ ,  $\kappa$  is the secondary scaling value,  $w^m$  and  $w^c$  are the weighted values and  $\xi$  is non-negative that combines the dynamic errors of higher order terms.

Step 3: Updating the state variables and estimation covariance in time domain and conducting the UT transformation again to generate new sigma points:

$$\begin{cases} \begin{bmatrix} x_{i,k|k-1} & \hat{x}_{k|k-1} & \bar{P}_{k|k-1} \end{bmatrix} = \left[ A_k x_{i,k-1} + B_k u_{k-1} + q_{k-1} \sum_{i=0}^{2L} w_m^{(i)} (x_{i,k|k-1} - \hat{x}_{k|k-1}) \bullet (x_{i,k|k-1} - \hat{x}_{k|k-1})^T + Q_{k-1} \right] \\ x_{i,k} = \left[ \hat{x}_{k|k-1} \quad \hat{x}_{k|k-1} + (\sqrt{(L+r)P_k^x})_i \quad \hat{x}_{k|k-1} - (\sqrt{(L+r)P_k^x})_{i-L} \right] \end{cases} \quad (20)$$

Step 4: Measurement update:

$$\begin{bmatrix} y_{i,k|k-1} & \hat{y}_{k|k-1} \end{bmatrix} = \left[ C_k x_{i,k} + D_k u_k + r_k \sum_{i=0}^{2L} w_i^m (y_{i,k|k-1}) \right] \quad (21)$$

Step 5: The estimation covariance and Kalman gain are updated as follows,

$$\begin{bmatrix} P_{yy,k} & P_{xy,k} & K_k \end{bmatrix} = \left[ \sum_{i=0}^{2L} w_i^c (y_{i,k|k-1} - \hat{y}_{k|k-1}) (y_{i,k|k-1} - \hat{y}_{k|k-1})^T + R_k \sum_{i=0}^{2L} w_i^c (x_{i,k|k-1} - \hat{x}_{k|k-1}) (y_{i,k|k-1} - \hat{y}_{k|k-1})^T P_{xy,k} \right] / P_{yy,k}$$

Step 6: Measurement correction of the state variables and updating of estimation covariance:

$$\begin{bmatrix} \hat{x}_k P_k \end{bmatrix} = \left[ \hat{x}_{k|k-1} + K_k (y_k - \hat{y}_{k|k-1}) \bar{P}_{k|k-1} - K_k \bar{P}_{yy,k} K_k^T \right] \quad (22)$$

Step 7: Updating the noises of the process and measurement:

$$\begin{cases} r_{k+1} = (1 - d_k) r_k + d_k \left[ v_k - \sum_{i=0}^{2L} w_i^m (y_{i,k|k-1}) \right] \\ R_{k+1} = (1 - d_k) R_k + d_k \left[ (v_k - \hat{y}_{k|k-1}) (v_k - \hat{y}_{k|k-1})^T \right] \\ q_{k+1} = (1 - d_k) q_k + d_k (\hat{x}_k - \hat{x}_k - q_k) \\ Q_{k+1} = (1 - d_k) Q_k + d_k \left( K_k (v_k - \hat{y}_{k|k-1}) (v_k - \hat{y}_{k|k-1})^T K_k^T + P_k \right) \\ d_k = \frac{(1-b)}{(1-b^k)} \end{cases} \quad (23)$$

where  $q$  is the mean of the system process noise,  $Q$  is the covariance of the process noise,  $r$  is the mean of the measurement noise and  $R$  is the covariance of the measurement noise.

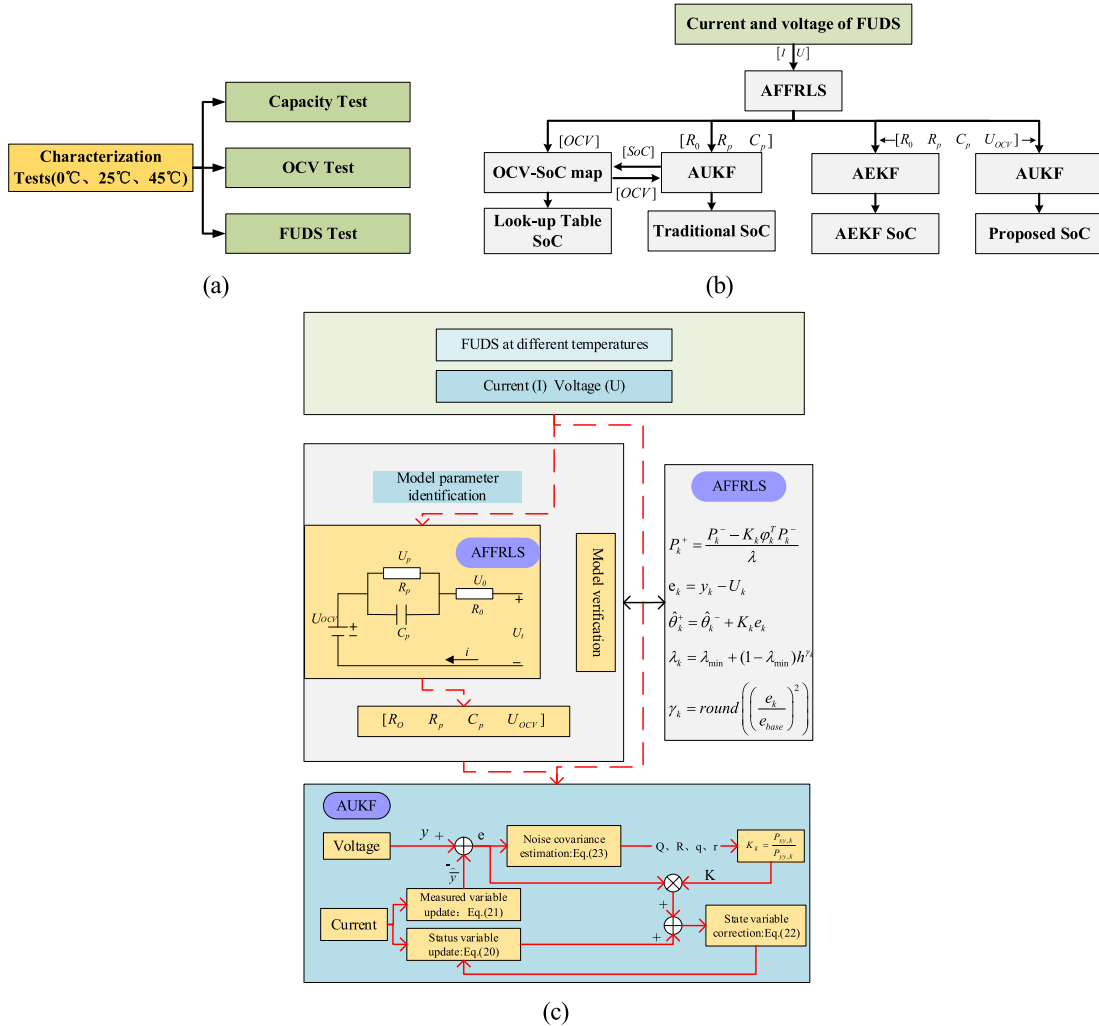


**Fig. 2.** (a) Battery experiments; (b) Comparison of SoC estimation; (c) Implementation of the proposed method.

### 1.2.2. ECM for the lithium-ion battery: parameters identification and OCV-SoC relationships

In general, there are mainly two types of model for the lithium-ion battery, i.e., the electrochemical model (EM) [33] and the ECM [8,34]. The EM uses the current, voltage and the concentration distribution of the conductive medium to describe the dynamic behavior of the lithium-ion battery. The EM is usually composed of a set of partial differential equations with plenty of unknown parameters [35], which is not easy to be solved although it has good accuracy. Consequently, the EM is difficult to be applied in the battery management system (BMS). In contrast, the ECM describes the dynamic and static characteristics of the battery with basic components such as capacitors and resistors, which is usually composed of an OCV, one or more RC circuits. It has been extensively used in the BMS due to its low complexity, low calculations.

The filter estimation method based on ECM has been widely used in the SoC estimation for lithium-ion batteries due to its closed-loop characteristics and considering various uncertainties. The commonly used filter algorithms include AEKF, AUKF, etc. It is requisite to identify the parameters of the ECMs to build the state space model for the SoC estimation. In [29,36] the AUKF is used to complete the SoC estimation based on a first-order RC ECM and second-order RC ECM, respectively. However, the parameters of the above models are identified offline, which cannot be applied under real time conditions [37]. To solve the poor real time problem resulted from the offline identification, the EKF is applied to identify the model parameters online [38], and the results show that it has a good identification accuracy, but the method involves

complex matrix transformation, which has a large computation. In [39] the recursive least square (RLS) method is put forward to update the model parameters in real time, and the SoC estimation is obtained using the UKF algorithm. However, the RLS algorithm tends to data saturation as time increases, which increases the SoC error. To deal with this issue, the forgetting factor has been incorporated to the RLS, which is called the forgetting factor RLS (FFRLS). In [32] the FFRLS is applied to recognize the model parameters, subsequently, the adaptive EKF (AEKF) is utilized to estimate the SoC, which significantly weakens the increasing trend of errors. However, since the forgetting factor is invariable, the accuracy and dynamic ability of the FFRLS will be influenced in case of frequently changing the charging or discharging currents. Consequently, in [40,41] the adaptive FFRLS (AFFRLS) is adopted to recognize the second-order RC model parameters online, of which the identification accuracy and real time characteristics of the AFFRLS have been verified by experiments. The above-mentioned methods have effectively improved the SoC estimation accuracy, but all the above methods require the SoC-OCV relationships.

The OCV is crucial for the ECM of the lithium-ion batteries, which has intrinsic relationship with the SoC. The low-current OCV (LO) [42] and incremental OCV (IO) [43,44] tests are mostly applied to obtain the OCV-SoC relationships offline. Under practical conditions, these two methods would take a long time and could be easily influenced by the environmental temperature and battery aging. Different OCV-SoC relationship curves could generate different influences on the real time SoC estimation [45]. In [43] the IO and LO experiments are researched at

**Table 4**  
Implementation processes and corresponding attributes of the four methods.

Method	Implementation process	Attributes
Look-up table	Step1: AFFRLS is utilized to identify the model parameters online. Step 2: The SoC is inferred from the offline OCV-SoC table with the identified OCV.	<ul style="list-style-type: none"> <li>• Open-loop method</li> <li>• Depending on the offline OCV-SoC tests</li> </ul>
Traditional AUKF	Step1: AFFRLS is utilized to identify the model parameters online. Step 2: The identified parameters except the OCV value are substituted into the state equation to calculate the priori SoC. Step 3: The OCV is inferred from the offline OCV-SoC table with the priori SoC. Step 4: The inferred OCV is substituted into the measurement equation to calculate the innovation to correct the priori SoC through the AUKF algorithm.	<ul style="list-style-type: none"> <li>• closed-loop method</li> <li>• Depending on the offline OCV-SoC tests</li> </ul>
AEKF	Step 1: AFFRLS is utilized to identify the model parameters including the OCV online. Step 2: The identified parameters except the OCV value are substituted into the state equation to calculate the priori SoC. Step 3: The identified OCV is substituted into the measurement equation to calculate the innovation to correct the priori SoC through the AEKF algorithm.	<ul style="list-style-type: none"> <li>• Closed-loop method</li> <li>• Without the offline OCV-SoC tests</li> <li>• Requiring derivative of the state equation and measurement equation to linearize the nonlinear system</li> </ul>
Proposed method	Step 1: AFFRLS is utilized to identify the model parameters including the OCV online. Step 2: The identified parameters are substituted into the state equation to calculate the priori SoC. Step 3: The identified OCV is substituted into the measurement equation to calculate the innovation to correct the priori SoC through the AUKF algorithm.	<ul style="list-style-type: none"> <li>• Closed-loop method</li> <li>• Without the offline OCV-SoC tests</li> <li>• It does not require linearize the nonlinear system</li> </ul>

three temperature conditions, confirming that the OCV-SoC relationships are influenced by the temperatures, in which the minimum difference between the two tests is observed at room temperature and there are larger differences at the other temperatures. In [46] the GPR is used to establish the complex relationships among the SoC, OCV, and temperature, and the results show that the proposed model could obtain more accurate SoC estimation at different temperatures, which takes a lot of time for collecting data and training the model. To reduce the time to attain the OCV-SoC relationship, various methods such as RLS [47,48], EKF [5], and H-infinity [44] have been used to obtain OCV values online without a long resting time. In [49] the OCV-SoC relationship are obtained from the working currents and voltages of a fully charged battery using an H infinity filter. In [50] the RLS is proposed to identify the parameters and OCV values for the circuit model, and then the Ah integral is adopted to attain the SoC, afterwards, the OCV values are correspondingly ordered to acquire the OCV-SoC relationship, and it is validated under different current conditions. The results reveal that the model accuracy is improved and the SoC estimation error is kept within 2 %, but the method should be carried out under constant current

or low current and it is more susceptible to the model parameters. With the increasing demand for real-time estimation of on-board power battery, many scholars take OCV as one of the battery parameters and use online identification method to dynamically acquire OCV. In [51] an adaptive estimation is used to obtain the model's parameters including the OCV based on the Thevenin ECM. The result shows the method has good accuracy. In [52] the AEKF is adopted to estimate OCV and other parameters, and then the identified OCV is leveraged to look up the OCV-SoC relationship, which shows the identified OCV can be applied to estimate the SoC with rational accuracy. In [5] an augmented EKF is used to jointly estimate the state variable and model parameters including the OCV and the result indicates the identified OCV has good precision. However, the augmented EKF has higher order thus easily leading to instability. In [53] the FFRLS is used to identify the parameters and the OCV, which is used to infer the SoC from the OCV-SoC table. The above methods require offline OCV tests to build the OCV-SoC relationship. However, offline OCV tests cost a lot of time, which is difficult to be applied to estimate the SoC online.

### 1.3. Main contributions

A closed-loop SoC estimation for the lithium-ion batteries is accomplished to void the offline OCV tests. The main contributions of this work are as follows:

- (1) The parameters including the OCV values for the lithium-ion battery are identified online by the AFFRLS based on its Thevenin model.
- (2) The SoC of the lithium-ion batteries is estimated by the AUKF without conducting OCV tests.
- (3) The relationships between the OCV and the SoC under different temperatures are reconstructed online.

The remainder of this paper is organized as follows: the Section 2 involves the methodologies used in this paper. In this section, the discrete form of the Thevenin model and the AFFRLS are introduced. The state and measurement equations for the lithium-ion battery are established, and the observability of the state variables is proved, based on which the AUKF is adopted to estimate the SoC. In Section 3 the model is validated, and the proposed method is compared with other three methods under different temperatures. Finally, the major conclusions are made.

## 2. Methodology

### 2.1. Battery modeling

Currently, the ECMs of the lithium-ion batteries are extensively used for the SoC estimation, such as the Rint model [54], the PNGV model [55], the Thevenin model and the second-order RC model [56]. Considering the model accuracy and calculation complexity, the Thevenin model is selected [57] in this paper. The Thevenin model is simple and can comprehensively simulate the dynamic and static performance of the battery, which can help reduce the calculation and improve the estimation accuracy.

The Thevenin model for the lithium-ion battery is depicted in Fig. 1. It comprises a voltage source  $U_{OCV}$ , a resistor  $R_0$ , and a  $R_p C_p$  parallel network. Herein,  $U_{OCV}$  is the OCV,  $R_0$  indicates the ohmic resistance,  $R_p$  represent the polarization resistance and  $C_p$  denotes the polarization capacitance,  $I_L$  is the working current,  $U_0$  denote the voltage across  $R_0$ ,  $U_t$  is the terminal voltage and  $U_p$  denote the polarization voltage across the  $R_p C_p$  parallel network, which describes the dynamic characteristics of the battery.

According to the Kirchhoff's law and after some formula derivation, the state equations of the Thevenin ECM can be obtained as follows:

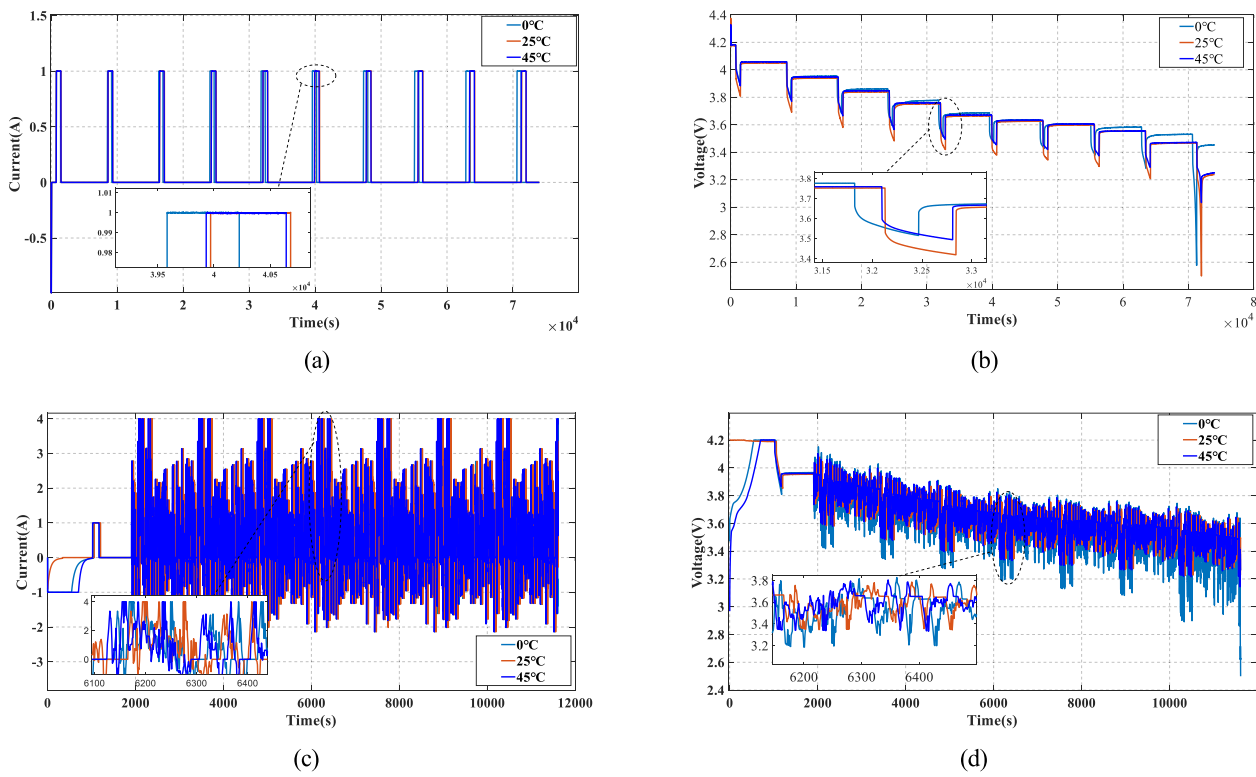


**Fig. 3.** (a) Current profile of IO; (b) Response voltage profile of IO; (c) Composed current profile of FUDS;

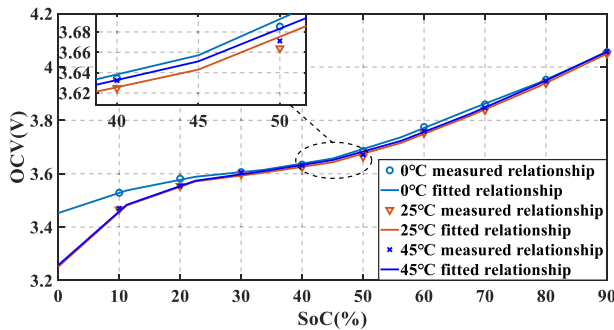


**Fig. 4.** OCV-SoC profiles at 0 °C, 25 °C and 45 °C.

$$\begin{cases} \dot{U}_p = -\frac{U_p}{C_p R_p} + \frac{I_L}{C_p} \\ U_t = U_{OCV} - U_p - I_L R_0 \end{cases} \quad (1)$$

Eq. (1) can be discretized as,

$$\begin{cases} U_{p,k} = U_{p,k-1} e^{-\frac{T_s}{C_p R_p}} + I_{L,k-1} R_p \left(1 - e^{-\frac{T_s}{C_p R_p}}\right) \\ U_{t,k} = U_{OCV,k} - U_{p,k} - I_{L,k} R_0 \end{cases} \quad (2)$$

where  $T_s$  is sampling interval, the subscripts  $k$  indicates the sampling moment and the  $U_{OCV}$  is the open circuit voltage related to temperatures, SoC and aging status.

From Eq. (2), the Laplace equation for the battery model can be deduced as,

$$E_t = U_t(s) - U_{OCV}(s) = -I_L(s) \left( \frac{R_p}{1 + C_p R_p s} \right) - I_L(s) R_0 \quad (3)$$

where  $E_t$  is defined as the difference between  $U_t$  and  $U_{OCV}$ , and  $s$  denotes the transfer function operator.

The transfer function of the battery model can be written as follows:

$$G_s = \frac{E_t(s)}{I_L(s)} = -R_0 - \frac{R_p}{1 + C_p R_p s} \quad (4)$$

Define  $s = \frac{2}{T_s} \frac{1-q^{-1}}{1+q^{-1}}$ , herein,  $q$  is the discretization factor. A bilinear transformation is applied for Eq. (4), and the results are shown in Eqs. (5) and (6):

$$G(q^{-1}) = -\frac{\beta_3 + \beta_4 q^{-1}}{1 - \beta_1 q^{-1}} \quad (5)$$

$$[\beta_1 \ \beta_3 \ \beta_4] = \left[ \begin{array}{ccc} \frac{1 - 2C_p R_p}{1 + 2C_p R_p} & \frac{R_0 + R_p + 2C_p R_p R_0}{1 + 2C_p R_p} & \frac{R_0 + R_p - 2C_p R_p R_0}{1 + 2C_p R_p} \end{array} \right] \quad (6)$$

The  $U_{OCV}$  can be considered as a slowly changing variable between the two adjacent sampling intervals [58]. Then Eq. (5) is arranged as,

$$U_{t,k} = \beta_1 U_{t,k-1} + (1 - \beta_1) U_{OCV,k} + \beta_3 I_{L,k} + \beta_4 I_{L,k-1} \quad (7)$$

Define  $\beta_2 = (1 - \beta_1) U_{OCV,k}$ ,  $\beta$  denotes the parameter variable to be identified.

## 2.2. Model identification based on AFFRLS

The RLS [49] is one of the most commonly used methods for parameter identification, which does not require a priori statistical knowledge and has small calculation. However, the RLS method encounters data saturation phenomenon in the identification process, thus influencing the identification accuracy. To deal with this issue, the AFFRLS is applied to identify the parameters in real time.

The standard form of the RLS algorithm is written as,

$$y_k = \varphi_k \theta_k^T + \varepsilon \quad (8)$$

where  $\varphi$  is a vector of the known information,  $\theta$  is a vector to be identified,  $\varepsilon$  is the random noise variable,  $y$  is the output of the system.

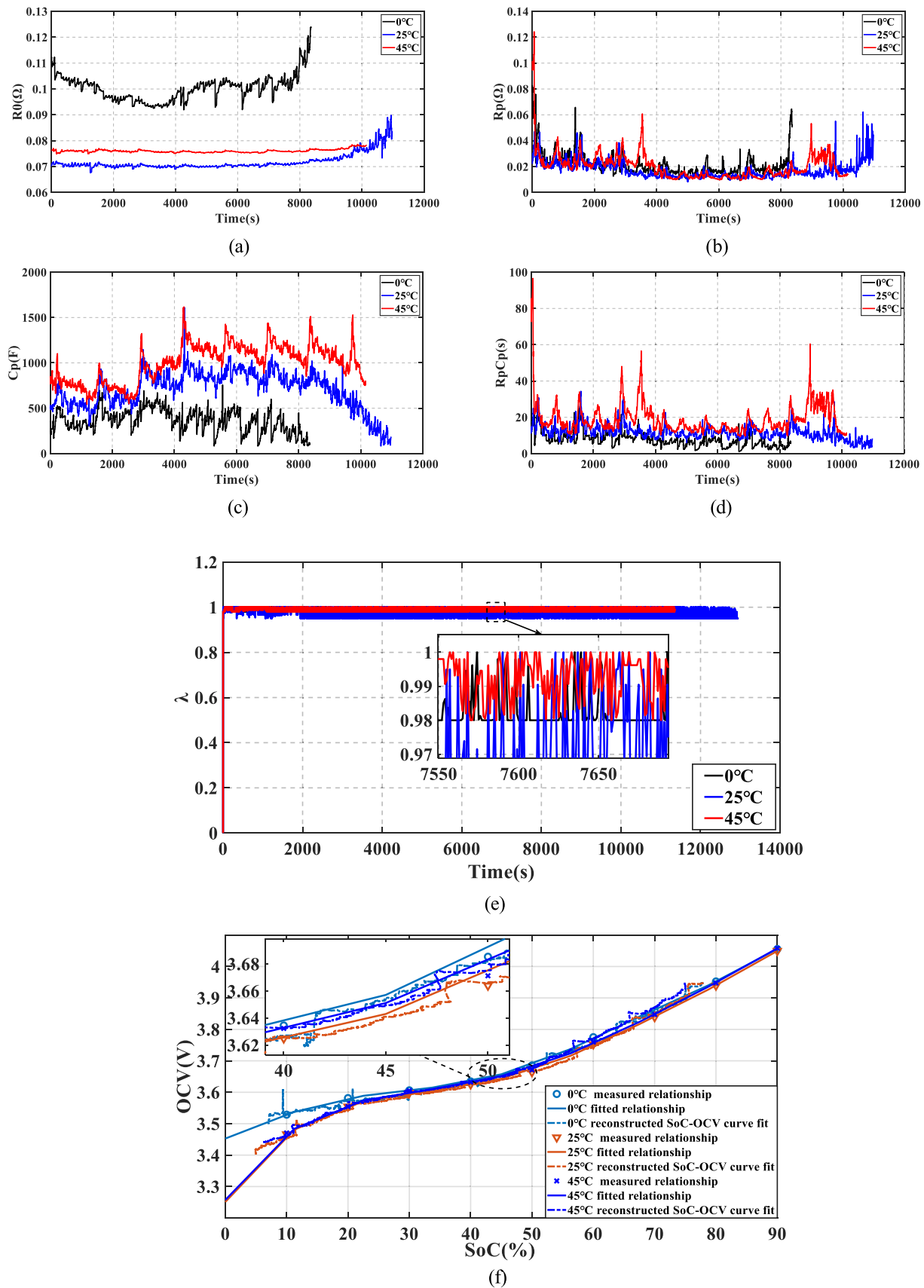


**Fig. 5.** Identification results at 0 °C, 25 °C and 45 °C (a)  $C_p$ ; (b)  $R_p$ ; (c)  $R_0$ ; (d)  $R_p C_p$ ; (e)  $\lambda$ ; (f) Reconstructed OCV- SoC relationships.

**Table 5**  
Model parameter identification at different temperatures.

Temperature	$R_0$ ( $\Omega$ )	$R_p$ ( $\Omega$ )	$C_p$ (F)
0 °C	0.0985	0.0199	373.7088
25 °C	0.0693	0.1797	760.1382
45 °C	0.0753	0.1898	984.9593

Comparing Eq. (7) and Eq. (8), we can get,

$$\begin{cases} \theta = [\beta_1 \quad \beta_2 \quad \beta_3 \quad \beta_4]^T \\ \varphi = [U_{t,k} \quad 1 \quad I_{L,k} \quad I_{L,k-1}] \end{cases} \quad (9)$$

where the Eq. (9) is solved with the AFFRLS.

The detailed implementation of AFFRLS are summarized in Table 2. Step 7 aims to adaptively update the forgetting factor  $\lambda$  as the identification error changes, so that the online identification has a faster convergence rate and a smaller identification error.  $\lambda_{\min}$  in Eq. (10) is the minimum value of the forgetting factor, and is chosen to be 0.98 making sure the parameters identification accurate and fast.  $h$  in Eq. (10) is the error sensitivity of the forgetting factor, and its range is [0– 1]. Considering the compromise between accuracy and rapidity of the identified parameters,  $h$  is selected to be 0.9.  $e_k$  in Eq. (10) denotes the sampling error at time and  $e_{base}$  is the allowable error reference value. The round ( $n$ ) denotes the closest integer to  $n$ . The Eq. (10) discloses that  $\lambda$  rapidly decreases when the error value  $e_k$  is higher than the reference error  $e_{base}$  at sampling time  $k$ . The  $e_{base}$  value is generally determined

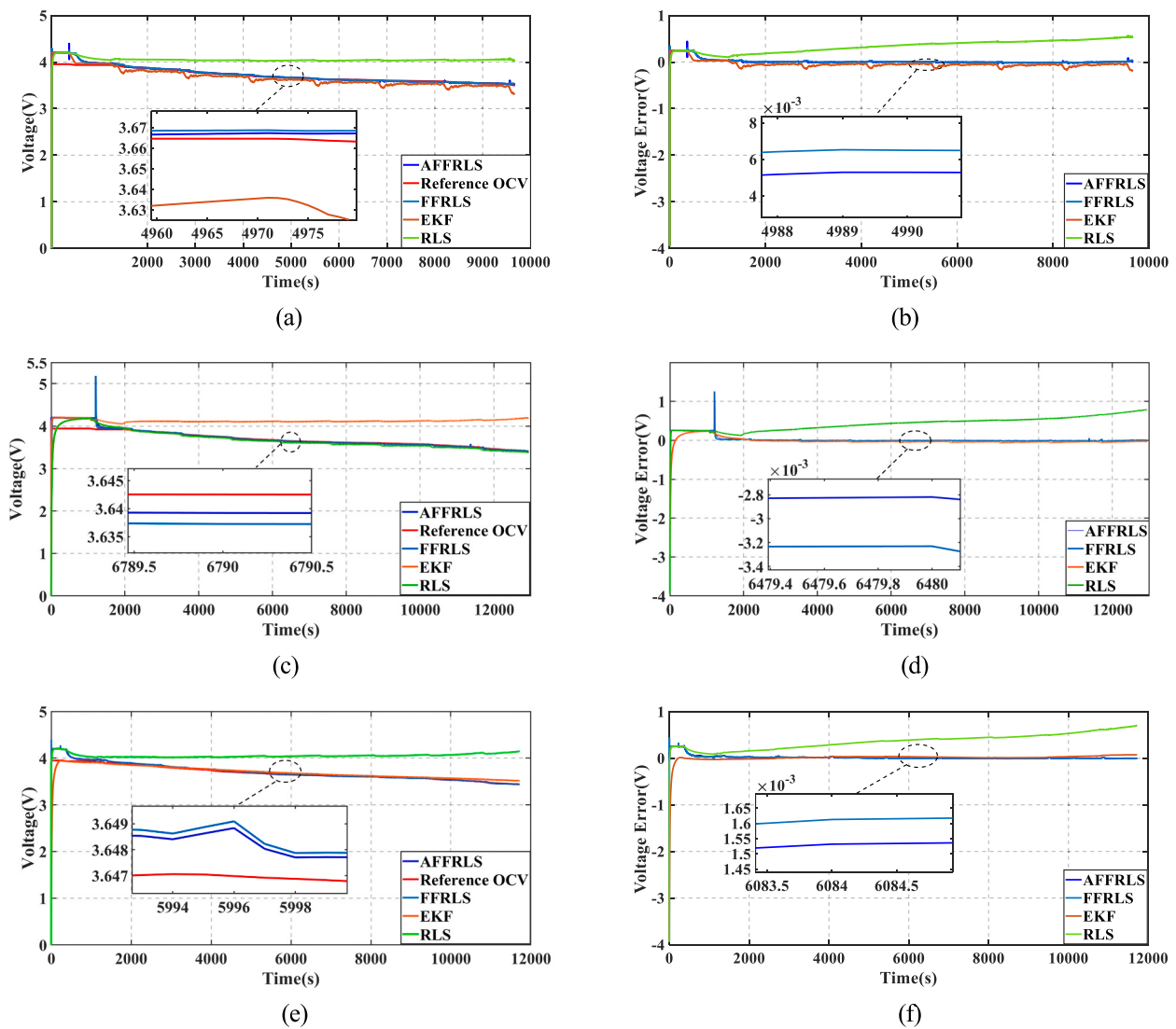


**Fig. 6.** Comparisons of identified OCVs and corresponding errors under different temperatures (a) identified OCVs at 0 °C (b) errors at 0 °C (c) identified OCVs at 25 °C (d) errors at 25 °C (e) identified OCVs at 45 °C (f) errors at 45 °C.

**Table 6**  
Error statistics of OCV identified by different methods.

Temperature	0 °C					25 °C					45 °C				
	A	F	E	R	A	F	E	R	A	F	E	R	A	F	E
Method <sup>a</sup>	A	F	E	R	A	F	E	R	A	F	E	R	A	F	E
MAE (%)	2.38	2.43	6.89	33.82	3.38	3.42	5.69	43.30	2.09	2.20	3.37	13.36			
RMSE (%)	0.52	0.53	0.84	13.04	0.78	0.97	1.44	21.42	0.37	0.40	1.20	15.97			

<sup>a</sup> A-AFFRLS;F-FFRLS;E-EKF;R-RLS.

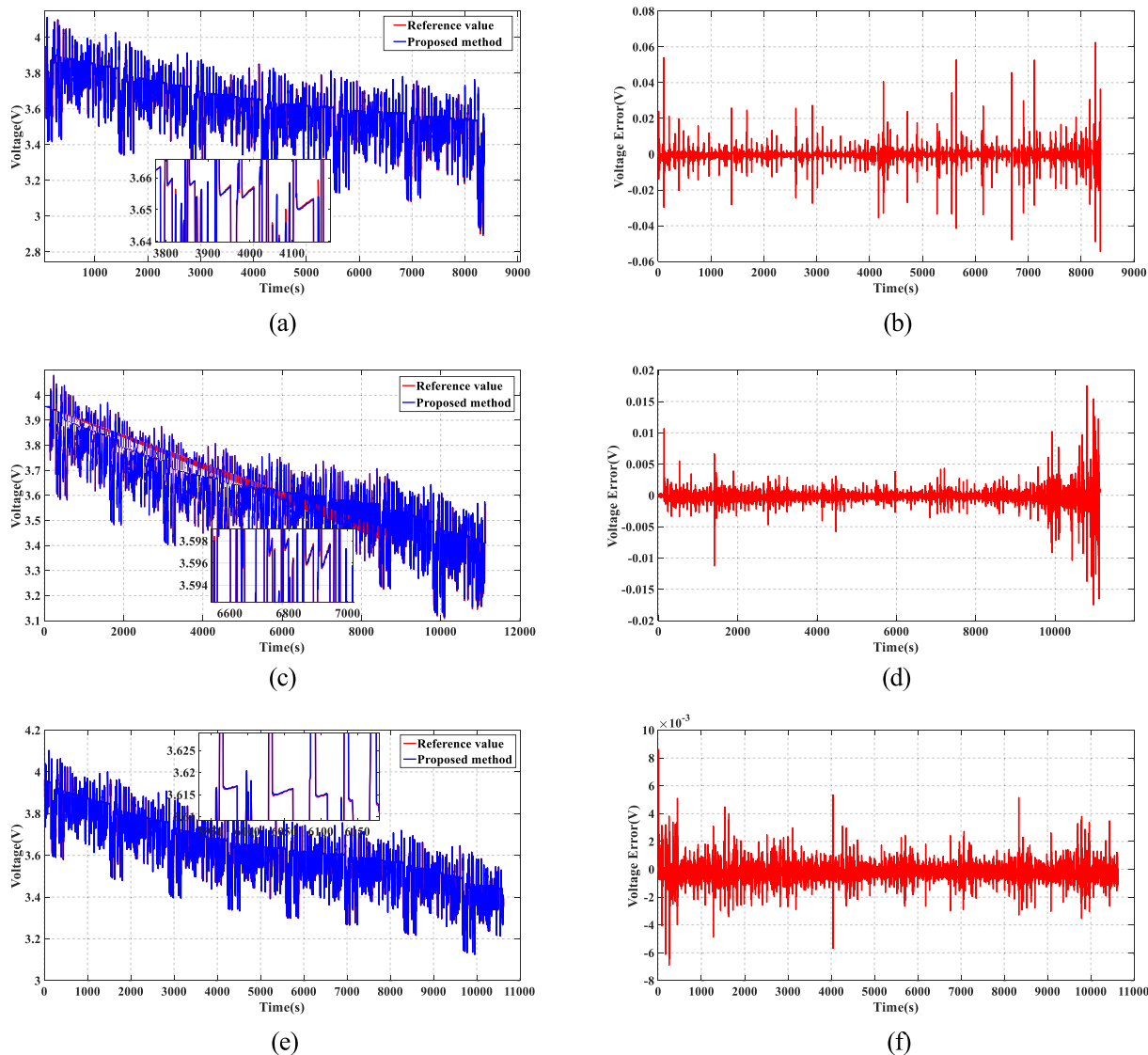


**Fig. 7.** Model validation under different temperatures: terminal voltages and corresponding errors at.

according to the expected error.

The parameter vector  $\theta$  can be identified through the AFFRLS, and then the parameters of the model can be derived according to Eq. (6). Define  $\tau = R_p C_p$ , the model parameters  $R_p$ ,  $C_p$ ,  $R_0$  and  $U_{OCV}$  can be reversely solved as Eq.(11):

$$[R_0 \ R_p \ C_p \ U_{OCV}] = \left[ \frac{(1+2\tau)(\beta_4 - \beta_3)}{4\tau} \ R_0(2\tau - 1) - \beta_4(1+2\tau) \ \frac{\tau}{R_p} \ \frac{\beta_2}{(1-\beta_1)} \right] \quad (11)$$

As can be seen from Eq. (11) when  $\beta_1 \neq 1$ , the OCV can be identified, and according to Eq. (6),  $\beta_1$  is not possibly equal to 1.

### 2.3. SOC estimation based on AUKF

#### 2.3.1. Observability of the state variables

At present, the model parameters are identified and the OCV values are attained online. In the traditional estimation method, the SoC are inferred from the OCV-SoC tables that are set up through offline OCV tests. This is a kind of open-loop method that cannot correct the estimation through a feedback mechanism. In addition, the OCV-SoC tables are influenced by the temperatures and aging, which means a large number of offline OCV tests should be performed to reflect these factors.

In this research, the identified OCV values are transmitted to an AUKF to accomplish a closed-loop SoC estimation, subsequently, the OCV-SoC relationships under different temperatures are reconstructed online.

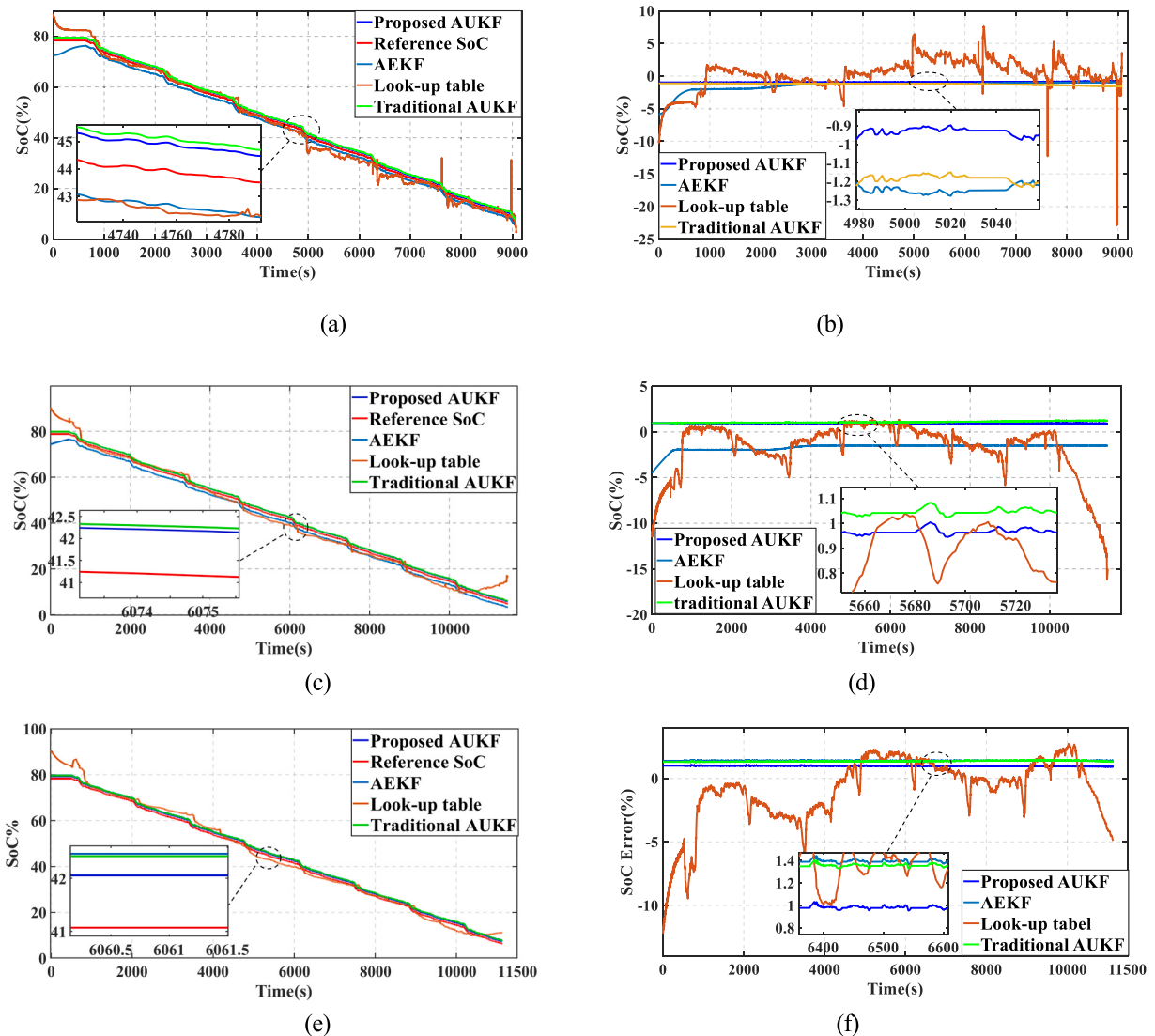
The SoC is usually defined as the ratio of the remaining capacity to the maximum capacity of a battery. And it is often expressed through the Ah integral method, which can be written as follows:

$$z = z_0 - \frac{\eta \int_0^t I dt}{C_n} \quad (12)$$

where  $z_0$  is the initial SoC,  $C_n$  is the nominal capacity and  $\eta$  is the Coulomb efficiency. The above equation can be discretized as:

$$z_k = z_{k-1} - \frac{\eta I_{k-1} T_s}{C_{n,k-1}} \quad (13)$$

According to the Thevenin model and combining with the Ah integral method, the polarization voltage and the SoC are selected as the state variables of the system, that is the  $x_k = [U_{p,k} \ z_k]^T$ . The state and measurement equations after discretization are written as follows:

**Fig. 8.** SOC estimation and corresponding errors under different temperatures.

(a) SOC estimation at 0 °C (b) errors at 0 °C; (c) SOC estimation at 25 °C (d) errors at 25 °C; (e) SOC estimation at 45 °C (f) errors at 45 °C.

**Table 7**

SOC estimation errors at 0 °C, 25 °C and 45 °C.

Temperature	0 °C				25 °C				45 °C			
Method <sup>a</sup>	U	E	T	L	U	E	T	L	U	E	T	L
MAE (%)	0.92	1.49	1.24	1.64	0.88	1.70	1.08	2.08	0.98	1.40	1.35	1.94
RMSE (%)	0.92	1.69	1.24	2.22	0.88	1.75	1.08	3.39	0.98	1.40	1.35	2.75

<sup>a</sup> U-AUKF; E-AEKF; T-Traditional AUKF; L-Look-up table.**Table 8**

Initial preset mean and variance of the noises for the AUKF at different temperatures.

	0 °C	25 °C	45 °C
R	0.01	0.01	0.1
r	0.01	0.01	0.1
Q	$\begin{bmatrix} 10^{-9} & 0 \\ 0 & 10^{-9} \end{bmatrix}$	$\begin{bmatrix} 10^{-6} & 0 \\ 0 & 10^{-9} \end{bmatrix}$	$\begin{bmatrix} 10^{-6} & 0 \\ 0 & 10^{-8} \end{bmatrix}$
q	$\begin{bmatrix} 10^{-3} \\ 10^{-2} \end{bmatrix}$	$\begin{bmatrix} 10^{-3} \\ 10^{-2} \end{bmatrix}$	$\begin{bmatrix} 10^{-1} \\ 10^{-2} \end{bmatrix}$

$$\begin{bmatrix} U_{p,k} \\ z_k \end{bmatrix} = \begin{bmatrix} e^{-\frac{T_s}{C_p R_p}} & 0 \\ 0 & 1 \end{bmatrix} \begin{bmatrix} U_{p,k-1} \\ z_{k-1} \end{bmatrix} + \begin{bmatrix} R_p \left(1 - e^{-\frac{T_s}{C_p R_p}}\right) \\ \frac{\eta T_s}{C_{n,k-1}} \end{bmatrix} I_{k-1} \quad (14)$$

$$U_{t,k} = U_{OCV,k} - U_{p,k} - I_{L,k} R_0 \quad (15)$$

where  $U_{OCV}$  is obtained through the AFFRLS.

According to Eqs. (1) and (9), the nonlinear system of the lithium-ion battery can be transformed into:

$$\begin{cases} \dot{x} = f(x) + gI_L \\ y = h(x) - R_0 I_L \end{cases} \quad (16)$$

		0 °C AUKF			25 °C AUKF			45 °C AUKF		
		90 % of preset values		110 % of preset values	90 % of preset values		110 % of preset values	90 % of preset values		110 % of preset values
R	0.0010	0.0010	0.0014	0.0015	0.0199	0.0015	0.0010	0.0207	0.0021	0.0021
r	0.0048	0.0053	0.0195	0.0195	[ -3.6 × 10 <sup>-22</sup> , 5.3 × 10 <sup>-8</sup> ]	[ -2.5 × 10 <sup>-25</sup> , 5.8 × 10 <sup>-8</sup> ]	[ 0.0617, -7.6 × 10 <sup>-25</sup> ]	[ 0.0975, 1.06 × 10 <sup>-23</sup> ]	[ 0.1192, 1.8 × 10 <sup>-22</sup> ]	[ 0.1192, 1.8 × 10 <sup>-22</sup> ]
Q	[ 3.2 × 10 <sup>-6</sup> , -6.6 × 10 <sup>-22</sup> ] [ -6.6 × 10 <sup>-22</sup> , 4.3 × 10 <sup>-8</sup> ]	[ 3.9 × 10 <sup>-6</sup> , -3.6 × 10 <sup>-22</sup> ] [ -3.6 × 10 <sup>-22</sup> , 5.3 × 10 <sup>-8</sup> ]	[ -2.4 × 10 <sup>-25</sup> , 5.8 × 10 <sup>-8</sup> ] [ -4 × 10 <sup>-323</sup> , -1.04 × 10 <sup>-6</sup> ]	[ -2.4 × 10 <sup>-25</sup> , 5.8 × 10 <sup>-8</sup> ] [ -4 × 10 <sup>-323</sup> , -1.04 × 10 <sup>-6</sup> ]	[ -7.6 × 10 <sup>-25</sup> , 7.1 × 10 <sup>-8</sup> ] [ -4 × 10 <sup>-323</sup> , -7.2 × 10 <sup>-6</sup> ]	[ -7.6 × 10 <sup>-25</sup> , 7.1 × 10 <sup>-8</sup> ] [ -4 × 10 <sup>-323</sup> , -7.2 × 10 <sup>-6</sup> ]	[ 1.1 × 10 <sup>-8</sup> , -1.2 × 10 <sup>-10</sup> ] [ -1.09 × 10 <sup>-7</sup> , -1.3 × 10 <sup>-7</sup> ]	[ 1.1 × 10 <sup>-8</sup> , -1.2 × 10 <sup>-10</sup> ] [ -1.09 × 10 <sup>-7</sup> , -1.3 × 10 <sup>-7</sup> ]	[ 1.8 × 10 <sup>-22</sup> , 1.4 × 10 <sup>-8</sup> ] [ -1.5 × 10 <sup>-110</sup> , -1.3 × 10 <sup>-7</sup> ]	[ 1.8 × 10 <sup>-22</sup> , 1.4 × 10 <sup>-8</sup> ] [ -1.5 × 10 <sup>-110</sup> , -1.3 × 10 <sup>-7</sup> ]
q	[ -4 × 10 <sup>-323</sup> ] [ -1.8 × 10 <sup>-7</sup> ]	[ -4 × 10 <sup>-323</sup> ] [ -2.4 × 10 <sup>-7</sup> ]	[ -4 × 10 <sup>-323</sup> ] [ -1.04 × 10 <sup>-6</sup> ]	[ -4 × 10 <sup>-323</sup> ] [ -1.04 × 10 <sup>-6</sup> ]	[ -4 × 10 <sup>-323</sup> ] [ -7.2 × 10 <sup>-6</sup> ]	[ -4 × 10 <sup>-323</sup> ] [ -7.2 × 10 <sup>-6</sup> ]	[ -4 × 10 <sup>-323</sup> ] [ -7.2 × 10 <sup>-6</sup> ]	[ -4 × 10 <sup>-323</sup> ] [ -7.2 × 10 <sup>-6</sup> ]	[ -4 × 10 <sup>-323</sup> ] [ -7.2 × 10 <sup>-6</sup> ]	[ -4 × 10 <sup>-323</sup> ] [ -7.2 × 10 <sup>-6</sup> ]

where the state variable  $x$  is  $[ U_p \ z ]^T$ , state function  $f(x)$  is  $\begin{bmatrix} -\frac{U_p}{\tau_p} & 0 \end{bmatrix}^T$ , input function  $g(x)$  is  $\begin{bmatrix} 1 \\ C_p \end{bmatrix}^T$ , measurement function  $h(x)$  is  $U_{OCV} - U_p$  and time constant  $\tau_p$  is  $C_p R_p$ .

The gradient of measurement function  $h$  to state variable  $x$  is:

$$dh = \frac{\partial h}{\partial x} = \begin{bmatrix} -1 & \frac{dU_{OCV}}{dz} \end{bmatrix} \quad (17)$$

Then the first order Lie derivates of  $h$  to  $f$  and  $g$  are:

$$\begin{cases} L_f h = dh \cdot f = \frac{U_p}{\tau_p} \\ L_g h = dh \cdot g = \left[ -1 \ \frac{dU_{OCV}}{dz} \right] \begin{bmatrix} 1 \\ C_p \end{bmatrix}^T = -\frac{1}{C_p} - \frac{\eta}{C_n} \frac{dU_{OCV}}{dz} \end{cases} \quad (18)$$

The observability at  $x_0$  [59] is determined by the observability matrix:

$$O(x_0) = \begin{bmatrix} dh \\ dL_f h \\ dL_g h \\ \vdots \end{bmatrix} = \begin{bmatrix} -1 & \frac{dU_{OCV}}{dz} \\ \frac{1}{\tau_p} & 0 \\ 0 & -\frac{\eta}{C_n} \frac{d^2 U_{OCV}}{dz^2} \\ \vdots & \vdots \end{bmatrix} \quad (19)$$

It is worth noting that  $\tau_p = C_p R_p$  is positive, so if there exists a  $k \in \mathbb{Z}^+$  where  $\mathbb{Z}$  denotes the positive integer such that  $\frac{d^k U_{OCV}}{dz^k}(x_0) \neq 0$ , the observability matrix has full rank at  $x_0$ , i.e., the rank  $n = 2$ . This means if all the derivatives of  $U_{OCV}$  against the SoC are not zero at the same time, the SoC can be locally observed at  $x_0$ . So, we can make the conclusion that the observability of the model determined by Eqs. (14) and (15) weakly depends on the nonlinearity of the  $U_{OCV}$  because no higher order derivatives of the  $U_{OCV}$  is required not to be zero. In addition, according to [59], this criterion of the local observability for the nonlinearity system is a sufficient condition.

### 2.3.2. SoC estimation based on AUKF

The UKF mainly utilizes a linear regression of  $n$  sigma points generated from the prior distribution to linearize the non-linear function of the random variables. Since UKF does not ignore higher order terms, the problems of poor stability and low accuracy of the EKF can be effectively overcome [48]. To decrease the uncertainties of the model and the system noises, the AUKF is adopted to estimate SoC, which can adaptively refresh the covariances of the process noise and the measurement noise in real time, thereby improving the SoC estimation accuracy. The estimation process of the AUKF is described in Table 3.

These steps are iterated to implement the AUKF algorithm. In contrast to the UKF, the AUKF adaptively updates the covariances of measurement noise and the process noise online, which can improve the estimation accuracy under unknown noise disturbance.

## 3. Experiment validation

### 3.1. The experiment setup

The 18650 LiNiMnCoO<sub>2</sub>/graphite lithium-ion battery is used in this experiment. The rated capacity of the battery is 2.0 Ah and the range of operating voltage is 2.5 V ~ 4.2 V. The batteries are tested at 0 °C, 25 °C and 45 °C. At each temperature, the capacity test, the IO test and the federal urban driving schedule (FUDS) test are conducted. The setup of the battery experiments is described in Fig. 2(a). The capacity test is performed at every selected temperature as follows: (1) the fully charged battery is discharged with 0.5C current until it reaches its charge cutoff

**Table 9**  
Final converged parameters of the AUKFs at different temperatures.

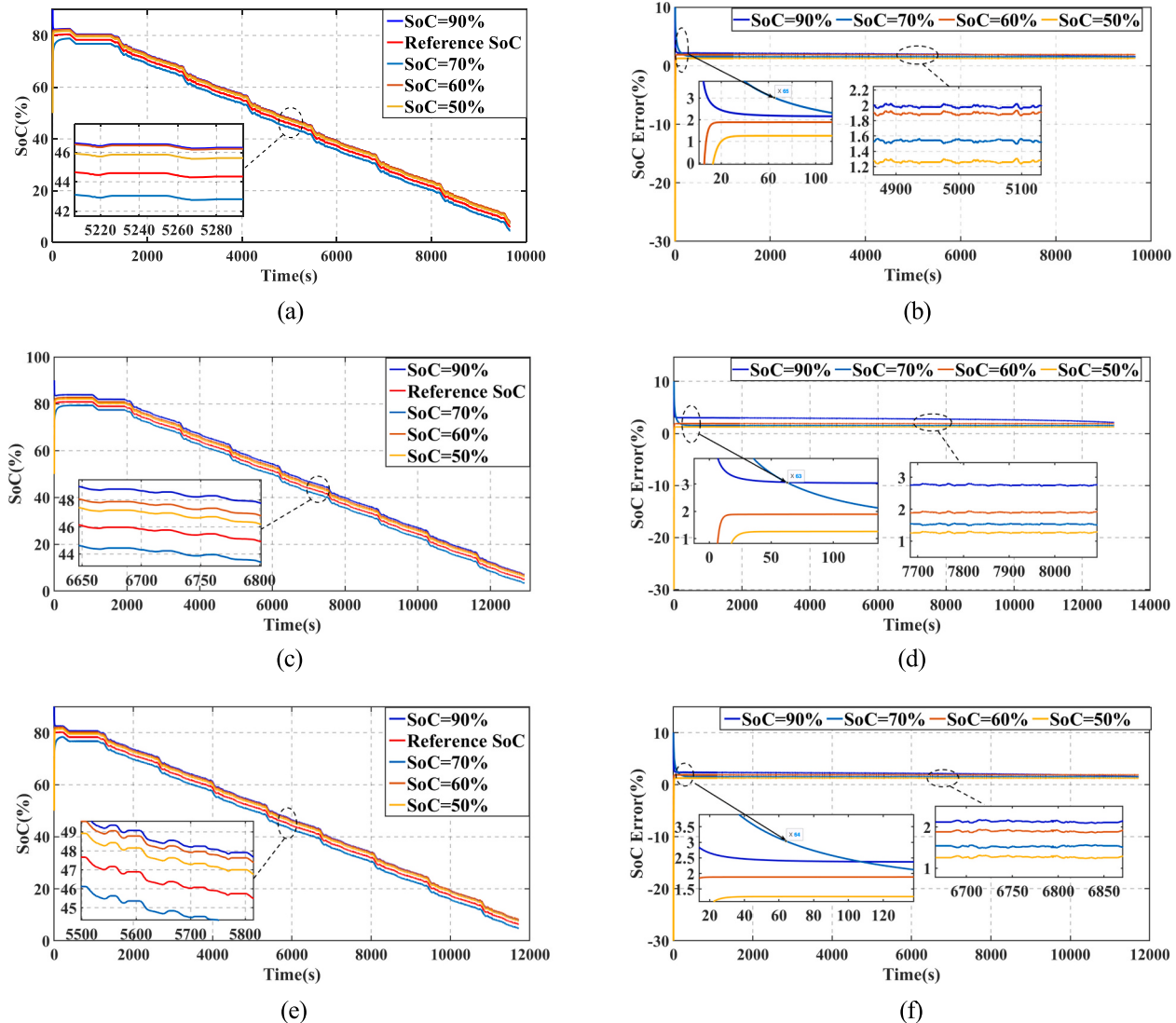


**Fig. 9.** Robustness of the SoC estimation to the initial values under different temperatures: (a) SoC estimation at 0 °C (b) estimation error at 0 °C; (c) SoC estimation at 25 °C; (d) estimation error at 25 °C; (e) SoC estimation at 45 °C; (f) estimation error at 45 °C.

voltage. Herein, the C indicates the rated capacity with the unit of Ah. (2) After resting for 2 h, the battery is charged with 0.5C current until it reaches its discharge cutoff voltage, (3) and then it is charged with constant voltage until the charge current falls to 0.05C, during which the quantity of delivered charge is considered as its capacity at this temperature.

The experiments are performed in the Center for Advanced Life Cycle Engineering (CALCE) at the University of Maryland [43] and the experimental data are adopted for this research. The experimental platform comprises a Vötsch programmable temperature chamber, an Arbin BT2000 battery charging/discharging test system and a host computer where the Arbin software is running for monitoring the charging/discharging process and recording the data.

The effectiveness of the proposed method is verified in comparison with three methods, i.e., the looking-up table method, the traditional AUKF method and the AEKF method, as depicted in Fig. 2(b). The looking-up method is an open-loop one, which directly looks up the SoC from the OCV-SoC table with the identified OCV. The traditional AUKF infers the OCV from the OCV-SoC relationship. Both the two methods need offline OCV tests to attain the OCV-SoC relationships, whereas the proposed AUKF method and the AEKF method do not need OCV tests, and they use the difference between the predicted terminal voltage and

the measured value to correct state variables to accomplish the closed-loop estimation. The implementation processes and corresponding attributes of these methods are shown in Table 4.

The proposed method is carried out as illustrated in Fig. 2(c). The whole process mainly consists of two parts. In the first part the battery parameters and OCV values are identified through the AFFRLS. The second part adopts AUKF to estimate the SoC with identified parameters and OCV values.

In this paper the IO test is used to validate the identified OCV values. The detailed test process is described as below: (1) The battery is fully charged and then rested for enough time so as to measure the OCV at its 100 % SoC. (2) The battery is discharged to its 90 % SoC with 0.5C current. Measure its current OCV after standing for 2 h. Repeat this step until the battery is fully discharged. The discharge voltage and current are shown in Fig. 3 (a) and Fig. 3 (b), respectively.

The proposed method is validated under the FUDS driving cycle. A single FUDS is 1372 s long. The battery current and its corresponding terminal voltage are shown in Fig. 3 (c) and (d), respectively, which consists of 8 FUDS driving cycles.

(d) Response voltage profile.

### 3.2. The fittings of the OCV and the SoC under different temperatures

The temperature affects the relationship between the OCV and SoC for the lithium-ion battery. Taking the strong nonlinearity into consideration, the OCV-SoC relationship is fitted with a sixth order polynomial as shown in Eq. (24), and the fitted and measured values are plotted in Fig. 4. As can be observed when the SoC is below 20 %, the difference of the OCV is a relatively significant (the maximum value is 60 mV) among the three temperatures. So, the effects of different temperatures on the OCV cannot be ignored when estimating the SoC.

$$V_{OCV}(z) = k_0(z)^6 + k_1(z)^5 + k_2(z)^4 + k_3(z)^3 + k_4(z)^2 + k_5(z) + k_6 \quad (24)$$

where  $k_i$ ,  $i \in [0, 6]$ , is the fitting coefficient.

### 3.3. Parameter identification results

The parameters including  $R_0$ ,  $C_p$ ,  $R_p$  are identified using the AFFRLS under the FUDS driving cycles. The identification results are plotted in Fig. 5(a), (b), (c). As can be observed, the internal resistances  $R_0$  at 0 °C are bigger than those of 25 °C and 45 °C. On the contrary, the values of the  $C_p$  at 0 °C are smaller than those of 25 °C and 45 °C. The time constant (That is the  $R_p \times C_p$ ) is the biggest at 45 °C temperature. The results reveal the parameters identified online can follow the change of the temperature. Through adaptive adjustment for the forgetting factor  $\lambda$ , the values of parameters change more steadily in the middle and later stages as the iteration process proceeds. The updating forgetting factor  $\lambda$  is shown in Fig. 5(e). From its local magnification, the forgetting factor  $\lambda$  changes adaptively with the input current, which enhances the dynamic identification ability.

It is worth noting that the identification lengths under different temperatures are different. The reason is that when the depth of discharging is the same, the cut-off voltages under different temperatures arrives at different time.

To reveal intuitive effect of temperature on model parameters, the mean values of the  $R_0$ ,  $R_p$  and  $C_p$  in the stable identification process are listed in Table 5. As can be seen from the table,  $R_p$  and  $C_p$  have a rising trend as the temperature increases and the  $C_p$  increases significantly. The resistance of  $R_0$  takes the maximum values at 0 °C. The identified parameters of  $R_p$ ,  $C_p$ ,  $R_0$  and  $U_{OCV}$  are updated in real time during the FUDS driving cycles, which makes the battery model adapt to dynamic conditions, enhancing the accuracy of the model.

The identified OCVs and reconstruct the OCV-SoC relationships under different temperatures are shown in Fig. 5(f), in which the local magnification shows that the identified OCVs are close to their references and the max error is less than 2 mV. The reference OCV values are obtained by inferring the OCV-SoC table based on the SoC value, which is obtained by Ah integral method. The OCV values identified by the AFFRLS are adopted to reconstruct the OCV-SoC relationships under different temperatures. As can be clearly observed, the reconstructed OCV-SoC curves almost coincide with the fitted curves under different temperatures, and the largest relative error is 0.59 % at 45 °C. It reveals that the identification of the OCV has high accuracy under different temperatures.

Since the OCV values identified online are utilized to estimate the SoC of the battery, the identified precision is particularly important. And the identified OCV values by the AFFRLS method are compared with those obtained by the FFRRLS, RLS and EKF methods, which are shown in Fig. 6. It can be observed that the identified OCV values by the AFFRLS are more accurate than those attained by the other three methods. The two commonly applied metrics of RMSE and MAE are adopted to evaluate the identified accuracy as listed in Table 6, and the mathematical expressions are shown in Eq. (25).

$$\left\{ \begin{array}{l} RMSE = \sqrt{\frac{1}{M} \sum_{k=1}^M (s_k - \hat{s}_k)^2} \\ MAE = \frac{1}{M} \sum_{k=1}^M |s_k - \hat{s}_k| \end{array} \right. \quad (25)$$

where  $M$  denotes samples number,  $s$  denotes the measured value, and  $\hat{s}$  presents the identified value.

### 3.4. Model validation

To verify the accuracy of the model, the identified model is evaluated by comparing the differences of the terminal voltage between the measured values and the output values of the model. The terminal voltages and corresponding terminal voltage errors under different temperatures are plotted in Fig. 7, where the blue curves represent the model output terminal voltages and red ones indicate the measured terminal voltages. As can be found that the estimated voltages obtained from the identified model are quite close to the measured values. The peak error occurs when the current changes suddenly, and the largest error occurs at 0 °C, and the largest absolute error is 6.25 mV and the relative error is less than 2 %. The results show that the identified model can well simulate the dynamic characteristics of the battery with high precision.

(a) terminal voltages at 0 °C (b) errors at 0 °C; (c) terminal voltages at 25 °C (d) errors at 25 °C; (e) terminal voltages at 45 °C (f) errors at 45 °C.

### 3.5. SoC estimation results

The proposed method as depicted in Fig. 2(c) utilizes the identified OCV to estimate the SoC with the AUKF. To validate the accuracy of the proposed method, it is compared with other methods for estimating the SoC as plotted in Fig. 2(b), where the look-up table method is an open-loop one and the other three methods are all closed-loop ones. The reference values are obtained by Ah integral method since the measured current has high precision and a tuning process is performed to calibrate the SoC initial value. As can be obtained from Fig. 8(a), (c) and (e) that the SoC curves estimated by the AUKF are closer to the reference than those of the other methods. The SoC errors estimated the closed-loop methods, which are more stable and less fluctuation when the SoC is below 10 %, are less than that estimated by the open-loop method at different temperatures. Among them, the SOC errors at 25 °C are less than those at 0 °C and 45 °C. The primary reason is that the errors of the estimated OCV values at 25 °C are less those at 0 °C and 45 °C, which can be observed form the reconstructed OCV-SoC relationships as shown in Fig. 5(f). In addition, the SoC error curves of the proposed methods has the least fluctuation in the whole process. One of the primary reasons is that the AUKF utilizes the unscented transformation to directly approximate the mean and covariance of the nonlinear system. It does not deal with solving the Jacobian matrix to linearize the nonlinear system, thus avoiding derivative and linearization errors. Besides, the proposed method is more accurate than the traditional AUKF.

Again, the RMSE and MAE are used to evaluate the estimation methods for the SoC. Table 7 lists the RMSE and MAE of the estimation errors. It can be found that the RMSE and MAE of the SoC error attained from the look-up table method, which is an open-loop estimation method, are larger than those of the other closed-loop methods. Among the closed-loop estimation methods, the MAE and RMSE values of the two AUKFs are less than those of the AEKF, in which the proposed AUKF is the smallest, indicating that it has better accuracy and stability for SoC estimation.

The initial parameter values of the KF are very important. Through a lot of experiments the initial means and variances of the noises are preset as listed in Table 8. Compared to the UKF, the AUKF can adaptively update the noises of the measurement and the process online, thus

improving the estimation accuracy. The convergence results of AUKF noises are shown in Table 9, where the initial mean and variance of the noises at different temperatures are adjusted to 110 % and 90 % of their preset values, and those parameters converge to rational range after multiple iterations. It can be observed from the table, the final converged values are close, which means that the parameters are updated to their true working conditions in real time.

### 3.6. Robustness analysis

In practical applications the initial SoC values are usually unknown. Therefore, those initial values are set to 50 %, 60 %, 70 % and 90 % to validate the robustness of the estimated SoC by the proposed AUKF. The results under different temperatures are plotted in Fig. 9. As can be observed, the proposed algorithm quickly converges to the references under different temperatures, no matter how far the initial values are set away from its true value, and the estimation errors can be kept less than 3 %. This reveals that the proposed method is robust to the initial SoC values under different temperatures.

## 4. Conclusion

In this paper, to void a large number of tests for modeling the lithium-ion battery and estimating its SoC, the closed-loop filter algorithm is proposed to estimate the SoC without conducting OCV tests under different temperatures. The discrete form of the Thevenin ECM for the lithium-ion battery is set up, based on which the AFFRLS is used to identify the model parameters and OCV values online. The observability of the state variables, i.e., the SoC and the polarization voltage, is proved through the Lie derivate analysis. The identified parameters and OCV values are substituted into the state function and the measurement equation and then the AUKF is leveraged to estimate the SoC. The OCV–SoC relationships under different temperatures are reconstructed in real time. The proposed method is validated under different temperatures. The research results show that this estimation method has high accuracy and fast convergence. In addition, it is robust to SoC initial values in wide temperature range.

In the future, the proposed method will be studied in aging condition to promote the algorithm into practice.

### CRediT authorship contribution statement

**Xiao Renxin:** Conceptualization, Methodology, Software, Writing – review & editing, Formal analysis. **Hu Yanwen:** Writing – original draft, Software, Investigation, Validation. **Zhang Wei:** Validation, Software. **Chen Zhaohui:** Supervision, Writing – review & editing.

### Declaration of competing interest

The authors declare that they have no known competing financial interests or personal relationships that could have appeared to influence the work reported in this paper.

### Data availability

The data that has been used is confidential.

### Acknowledgments

This work was supported by Yunnan Ten Thousand Talents Plan Young & Elite Talents Project (Grant No. KKRD201902062).

## References

- [1] K. Yang, Y. Tang, Z. Zhang, Parameter identification and state-of-charge estimation for lithium-ion batteries using separated time scales and extended Kalman filter, *Energies* 14 (4) (2021).
- [2] Y. Fan, H. Shi, S. Wang, C. Fernandez, W. Cao, J. Huang, A novel adaptive Function—Dual Kalman filtering strategy for online battery model parameters and state of charge co-estimation, *Energies* 14 (8) (2021).
- [3] N. Peng, S. Zhang, X. Guo, X. Zhang, Online parameters identification and state of charge estimation for lithium-ion batteries using improved adaptive dual unscented Kalman filter, *Int. J. Energy Res.* 45 (1) (2020) 975–990.
- [4] Y. Song, M. Park, M. Seo, S.W. Kim, Online state-of-charge estimation for lithium-ion batteries considering model inaccuracies under time-varying current conditions, *IEEE Access* 8 (2020) 192419–192434.
- [5] F. Feng, R. Lu, G. Wei, C. Zhu, Online estimation of model parameters and state of charge of LiFePO4 batteries using a novel open-circuit voltage at various ambient temperatures, *Energies* 8 (4) (2015) 2950–2976.
- [6] Y. Chen, G. Yang, X. Liu, Z. He, A time-efficient and accurate open circuit voltage estimation method for lithium-ion batteries, *Energies* 12 (9) (2019).
- [7] L. Kang, X. Zhao, J. Ma, A new neural network model for the state-of-charge estimation in the battery degradation process, *Appl. Energy* 121 (2014) 20–27.
- [8] R. Xiong, J. Tian, H. Mu, C. Wang, A systematic model-based degradation behavior recognition and health monitoring method for lithium-ion batteries, *Appl. Energy* 207 (2017) 372–383.
- [9] X. Dang, L. Yan, H. Jiang, X. Wu, H. Sun, Open-circuit voltage-based state of charge estimation of lithium-ion power battery by combining controlled auto-regressive and moving average modeling with feedforward-feedback compensation method, *Int. J. Electr. Power Energy Syst.* 90 (2017) 27–36.
- [10] F. Leng, C.M. Tan, R. Yazami, M.D. Le, A practical framework of electrical based online state-of-charge estimation of lithium ion batteries, *J. Power Sources* 255 (2014) 423–430.
- [11] N. Yang, X. Zhang, G. Li, State of charge estimation for pulse discharge of a LiFePO4 battery by a revised ah counting, *Electrochim. Acta* 151 (2015) 63–71.
- [12] R. Xiong, H. He, F. Sun, K. Zhao, Evaluation on state of charge estimation of batteries with adaptive extended Kalman filter by experiment approach, *IEEE Trans. Veh. Technol.* 62 (1) (2013) 108–117.
- [13] H.W. He, R. Xiong, H.Q. Guo, Online estimation of model parameters and state-of-charge of LiFePO4 batteries in electric vehicles, *Appl. Energy* 89 (1) (2012) 413–420.
- [14] T. Weigert, Q. Tian, K. Lian, State-of-charge prediction of batteries and battery-supercapacitor hybrids using artificial neural networks, *J. Power Sources* 196 (8) (2011) 4061–4066.
- [15] X. Zhao, D. Xuan, K. Zhao, Z. Li, Elman neural network using ant colony optimization algorithm for estimating of state of charge of lithium-ion battery, *J. Energy Storage* 32 (2020).
- [16] W. Duan, C. Song, S. Peng, F. Xiao, Y. Shao, S. Song, An improved gated recurrent unit network model for state-of-charge estimation of lithium-ion battery, *Energies* 13 (23) (2020).
- [17] X. Ren, S. Liu, X. Yu, X. Dong, A method for state-of-charge estimation of lithium-ion batteries based on PSO-LSTM, *Energy* 234 (2021).
- [18] X. Feng, J. Chen, Z. Zhang, S. Miao, Q. Zhu, State-of-charge estimation of lithium-ion battery based on clockwork recurrent neural network, *Energy* 236 (2021).
- [19] J.C. Alvarez Anton, P.J. Garcia Nieto, C. Blanco Viejo, J.A. Vilan Vilan, Support vector machines used to estimate the battery state of charge, *IEEE Transactions on Power Electronics* 28 (12) (2013) 5919–5926.
- [20] D. Andre, C. Appel, T. SoCzka-Guth, D.U. Sauer, Advanced mathematical methods of SOC and SOH estimation for lithium-ion batteries, *J. Power Sources* 224 (2013) 20–27.
- [21] X. Dang, L. Yan, K. Xu, X. Wu, H. Jiang, H. Sun, Open-circuit voltage-based state of charge estimation of Lithium-ion battery using dual neural network fusion battery model, *Electrochim. Acta* 188 (2016) 356–366.
- [22] M.A. Hannan, M.S.H. Lipu, A. Hussain, M.H. Saad, A. Ayob, Neural network approach for estimating state of charge of lithium-ion battery using backtracking search algorithm, *IEEE Access* 6 (2018) 10069–10079.
- [23] J. Meng, G. Luo, F. Gao, Lithium polymer battery state-of-charge estimation based on adaptive unscented Kalman filter and support vector machine, *IEEE Trans. Power Electron.* 31 (3) (2016) 2226–2238.
- [24] B. Ning, J. Xu, B. Cao, B. Wang, G. Xu, A sliding mode observer SOC estimation method based on parameter adaptive battery model, *Energy Procedia* 88 (CENCON) (2016) 619–626.
- [25] S. Wang, D.-I. Stroe, C. Fernandez, C. Yu, C. Zou, X. Li, A novel energy management strategy for the ternary lithium batteries based on the dynamic equivalent circuit modeling and differential Kalman filtering under time-varying conditions, *J. Power Sources* 450 (2020).
- [26] M. Al-Gablawy, N.S. Hosny, J.A. Dawson, A.I. Omar, State of charge estimation of a li-ion battery based on extended Kalman filtering and sensor bias, *Int. J. Energy Res.* 45 (5) (2020) 6708–6726.
- [27] L. Zhi, Z. Peng, W. Zhifu, S. Qiang, R. Yinan, State of charge estimation for li-ion battery based on extended Kalman filter, *Energy Procedia* 105 (2017) 3515–3520.
- [28] J. Li, M. Ye, S. Jiao, W. Meng, X. Xu, A novel state estimation approach based on adaptive unscented Kalman filter for electric vehicles, *IEEE Access* 8 (2020) 185629–185637.
- [29] E.G. Hou, X. Qiao, G.M. Liu, SOC estimation for Power Lithium-ion Battery Based on AUKF, in: H. Davis, Z.G. Fang, J.F. Ke (Eds.), *Proceedings of the 2016 International Conference on Artificial Intelligence and Engineering Applications*, Atlantis Press, Paris, 2016, pp. 14–18.

- [30] A. Alkaya, Unscented Kalman filter performance for closed-loop nonlinear state estimation: a simulation case study, *Electr. Eng.* 96 (4) (2014) 299–308.
- [31] W. Duan, C. Song, Y. Chen, F. Xiao, S. Peng, Y. Shao, S. Song, Online parameter identification and state of charge estimation of battery based on multimescale adaptive double Kalman filter algorithm, *Math. Probl. Eng.* 2020 (2020).
- [32] X. Guo, L. Kang, Y. Yao, Z. Huang, W. Li, Joint estimation of the electric vehicle power battery state of charge based on the least squares method and the Kalman filter algorithm, *Energies* 9 (2) (2016).
- [33] M.A. Rahman, S. Anwar, A. Izadian, Electrochemical model parameter identification of a lithium-ion battery using particle swarm optimization method, *J. Power Sources* 307 (2016) 86–97.
- [34] Y. Zou, X. Hu, H. Ma, S.E. Li, Combined state of charge and state of health estimation over lithium-ion battery cell cycle lifespan for electric vehicles, *J. Power Sources* 273 (2015) 793–803.
- [35] X. Han, Z. Wang, Z. Wei, A novel approach for health management online-monitoring of lithium-ion batteries based on model-data fusion, *Appl. Energy* 302 (2021).
- [36] J. Lv, B. Jiang, X. Wang, Y. Liu, Y. Fu, Estimation of the state of charge of lithium batteries based on adaptive unscented Kalman filter algorithm, *Electronics* 9 (9) (2020).
- [37] L. He, M. Hu, Y. Wei, B. Liu, Q. Shi, State of charge estimation by finite difference extended Kalman filter with HPPC parameters identification, *Sci. China Technol. Sci.* 63 (3) (2020) 410–421.
- [38] C. Hu, B.D. Youn, J. Chung, A multiscale framework with extended Kalman filter for lithium-ion battery SOC and capacity estimation, *Appl. Energy* 92 (2012) 694–704.
- [39] M. Oya, W. Sueki, Y. Hayakawa, K. Takaba, M. Fukui, S. Electrochem, in: Combined RLS-EKF Method for Simultaneous SOC and Parameter Estimations for Lithium-ion Batteries, Selected Proceedings From the 232nd Ecs Meeting, 2017, pp. 207–217.
- [40] X. Sun, J. Ji, B. Ren, C. Xie, D. Yan, Adaptive forgetting factor recursive Least Square algorithm for online identification of equivalent circuit model parameters of a lithium-ion battery, *Energies* 12 (12) (2019).
- [41] E. Mouncef, B. Mostafa, E. Naoufi, Online parameter estimation of an electric vehicle lithium-ion battery using AFFRLs, in: 2020 IEEE 2nd International Conference on Electronics, Control, Optimization and Computer Science (ICECOCS), 2020, pp. 1–6.
- [42] Q.-Q. Yu, R. Xiong, L.-Y. Wang, C. Lin, A comparative study on open circuit voltage models for Lithium-ion batteries, *Chin. J. Mech. Eng.* 31 (1) (2018).
- [43] F. Zheng, Y. Xing, J. Jiang, B. Sun, J. Kim, M. Pecht, Influence of different open circuit voltage tests on state of charge online estimation for lithium-ion batteries, *Appl. Energy* 183 (2016) 513–525.
- [44] C. Lin, Q. Yu, R. Xiong, L.Y. Wang, A study on the impact of open circuit voltage tests on state of charge estimation for lithium-ion batteries, *Appl. Energy* 205 (2017) 892–902.
- [45] A. Gismero, D.-I. Stroe, E. Schaltz, Ieee, Comparative study of state of charge estimation under different open circuit voltage test conditions for lithium-ion batteries, in: Iecon 2020: The 46th Annual Conference of the Ieee Industrial Electronics SoCiety, 2020, pp. 1767–1772.
- [46] C. Huang, L. Wang, Gaussian process regression-based modelling of lithium-ion battery temperature-dependent open-circuit-voltage, *Electron. Lett.* 53 (17) (2017) 1214–1216.
- [47] D. Van-Huan, H.A. Bastawrous, K. Lim, K.W. See, P. Zhang, S.X. Dou, Online state of charge and model parameters estimation of the LiFePO<sub>4</sub> battery in electric vehicles using multiple adaptive forgetting factors recursive least-squares, *J. Power Sources* 296 (2015) 215–224.
- [48] D. Kong, S. Wang, P. Ping, A novel parameter adaptive method for state of charge estimation of aged lithium batteries, *J. Energy Storage* 44 (2021).
- [49] C. Zhang, W. Allafi, Q. Dinh, P. Ascencio, J. Marco, Online estimation of battery equivalent circuit model parameters and state of charge using decoupled least squares technique, *Energy* 142 (2018) 678–688.
- [50] Y. Song, M. Park, M. Seo, S.W. Kim, Improved SOC estimation of lithium-ion batteries with novel SOC-OCV curve estimation method using equivalent circuit model, 2019.
- [51] Y.-H. Chiang, W.-Y. Sean, J.-C. Ke, Online estimation of internal resistance and open-circuit voltage of lithium-ion batteries in electric vehicles, *J. Power Sources* 196 (8) (2011) 3921–3932.
- [52] H. He, R. Xiong, H. Guo, Online estimation of model parameters and state-of-charge of LiFePO<sub>4</sub> batteries in electric vehicles, *Appl. Energy* 89 (1) (2012) 413–420.
- [53] Z. Shuzhi, G. Xu, Z. Xiongwen, A novel one-way transmitted co-estimation framework for capacity and state-of-charge of lithium-ion battery based on double adaptive extended Kalman filters, *Journal of Energy Storage* 33 (2021).
- [54] J. Yang, X.Z. Wei, H.F. Dai, J.G. Zhu, X.D. Xu, Ieee, Lithium-ion Battery Internal Resistance Model Based on the Porous Electrode Theory, Ieee, New York, 2014.
- [55] R. Xiao, J. Shen, X. Li, W. Yan, E. Pan, Z. Chen, Comparisons of modeling and state of charge estimation for lithium-ion battery based on fractional order and integral order methods, *Energies* 9 (3) (2016).
- [56] B.Y. Liaw, G. Nagasubramanian, R.G. Jungst, D.H. Doughty, Modeling of lithium ion cells - a simple equivalent-circuit model approach, *Solid State Ionics* 175 (1–4) (2004) 835–839.
- [57] X. Hu, S. Li, H. Peng, A comparative study of equivalent circuit models for Li-ion batteries, *J. Power Sources* 198 (2012) 359–367.
- [58] H. He, R. Xiong, H. Guo, S. Li, Comparison study on the battery models used for the energy management of batteries in electric vehicles, *Energy Convers. Manag.* 64 (2012) 113–121.
- [59] S. Zhao, S.R. Duncan, D.A. Howey, Observability analysis and state estimation of lithium-ion batteries in the presence of sensor biases, *IEEE Trans. Control Syst. Technol.* 25 (1) (2017) 326–333.